ARTICLE OPEN

Check for updates

CMKLR1/PKA signaling reinforces sonic hedgehog pathway to promote medulloblastoma pathogenesis

Shan Wang[1,2,7], Tongtong Jiang[2,7], Tao Wang[3,7], Zhiwei Yang[4,7], Ting Wang[2], Xiao Zhang[2], Xingchun Gou[1], Lintao Jia[2✉], Liang Wang[5✉] and Yang Song[6✉]

Aberrant Hedgehog signaling is a key driver of malignancies like medulloblastoma (MB), the most common pediatric brain tumor originating from cerebellar granule neuron progenitors with largely uncharacterized mechanisms. We found here that the G protein-coupled receptor, chemokine-like receptor 1 (CMKLR1), is upregulated and correlates with the development of Sonic Hedgehog (SHH)-subtype MB. SHH and the downstream transcription factor Gli2 license the expression of CMKLR1, which promotes the growth and migration of cells by activating Gα(i)βγ and subsequently the PI3K/Akt signal pathway. SHH/Gli also transcriptionally represses Regulator of G Protein Signaling 16 (RGS16), a known suppressor of Gα(i). Meanwhile, CMKLR1/Gα(i) signaling inactivates protein kinase A (PKA), reduces PKA-catalyzed phosphorylation of Gli2, and circumvents its proteasomal degradation, thus forming a feedback circuit in medulloblastoma cells. Consistently, CMKLR1 ablation suppresses the in vivo development of SHH subtype MB, which is counteracted by further silencing of the PKA catalytic subunit. These findings provide novel insights into the oncogenic network of Hedgehog pathway-driven cancer.

Oncogenesis (2025)14:40 ; https://doi.org/10.1038/s41389-025-00582-1

INTRODUCTION

Hedgehog signaling is a crucial pathway of ontogenesis that controls cell growth, survival and fate in divergent tissues [1, 2]. In the absence of an activating ligand such as SHH, the antagonizing receptor Patched1 (Ptch1) inhibits the activity of the multipass transmembrane protein Smoothened (Smo) [1]. Binding of SHH to Ptch1 releases Smo and results in the activation of downstream transcription factors including Gli1, Gli2 and Gli3 [1, 2]. These factors, which are otherwise constitutively degraded or alternatively processed, convert the signals into transcription or repression (in case of Gli3) of a cohort of genes involved in various physiological processes [3]. The degradation of Gli2/3 via the ubiquitin-proteasome pathway has been found to require phosphorylation, primarily mediated by protein kinase A (PKA) [4]. In contrast to its indispensable roles in embryonic development and maintenance of tissue homeostasis, excessive activation of the Hedgehog signaling is associated with several human malignancies [5, 6]. However, the key players downstream of the SHH pathway and the target genes of Gli family transcription factor that mediate MB development remain largely elusive [5].

Medulloblastoma (MB) represents the most common pediatric malignancy in the central nervous system, accounting for 20% of all childhood brain tumors [7]. Although arising from the cerebellum, particularly cerebellar granule neuron precursor cell (CGNPs) in this region, MB can grow rapidly and spread (or metastasize) to other parts of the brain or spinal cord [7, 8]. While it is histologically heterogeneous, MB can be classified into 4 molecular subtypes based on varied driver gene mutations and transcriptional profiles: Sonic Hedgehog (SHH), Wingless (Wnt), Groups 3 and 4 [9]. SHH subgroup tumors make up approximately 27% of all MBs, and are found most commonly in adults and infants [9]. In these malignancies, somatic mutations were detected most frequently in genes encoding Ptch1, Smo, and Suppressor of Fused (Sufu), a key repressor of Hedgehog signaling [10]. The incidence of CNS metastatic disease in the SHH subgroup at diagnosis is relatively common, and the prognosis remains to be improved due to lack of targeted treatment in addition to surgery, necessitating the exploration of classical Hedgehog pathway-centered network that underlies MB pathogenesis [9, 10].

Chemokine-like receptor 1 (CMKLR1/ChemR23) is the major receptor of chemerin, a multifunctional adipokine with established roles in inflammation, metabolism and other cellular processes [11]. As a G protein-coupled receptor, its engagement by the ligand triggers activation of protein kinases like Syk and Src, and evokes intracellular signaling via canonical PI3K/Akt and Ras/MAPK pathways [12]. The hyperactivity of chemerin/CMKLR1 signaling is also widely implicated in various pathological conditions including cancer [13]. Although chemerin was reported to suppress carcinogenesis most likely via recruiting innate immune cells, accumulating evidence has demonstrated its oncogenic roles via autonomous or autocrine CMKLR1 signaling in cancer cells [13, 14]. High serum chemerin levels or CMKLR1

[1]Institute of Basic and Translational Medicine, Xi'an Medical University, Xi'an, Shaanxi, China. [2]State Key Laboratory of Cancer Biology, Department of Biochemistry and Molecular Biology, Fourth Military Medical University, Xi'an, Shaanxi, China. [3]Department of Neurology, Shaanxi Provincial People's Hospital, Xi'an, Shaanxi, China. [4]MOE Key Laboratory for Nonequilibrium Synthesis and Modulation of Condensed Matter, School of Physics, Xi'an Jiaotong University, Xi'an, Shaanxi, China. [5]Department of Neurosurgery, Tangdu Hospital, Fourth Military Medical University, Xi'an, Shaanxi, China. [6]Department of Oncology, Tangdu Hospital, Fourth Military Medical University, Xi'an, Shaanxi, China. [7]These authors contributed equally: Shan Wang, Tongtong Jiang, Tao Wang, Zhiwei Yang. ✉email: jialth@fmmu.edu.cn; drwangliang@126.com; songyang212212@163.com

Received: 21 March 2025 Revised: 19 September 2025 Accepted: 30 September 2025
Published online: 17 November 2025

expression in tumor tissues has been demonstrated to correlate with poor prognosis of gastric, breast and colorectal cancers [15]. However, studies on factors or pathways that lead to aberrant chemerin/CMKLR1 signaling during tumorigenesis are so far limited, and how it responds to documented cancer-driving molecular events remains obscure [13, 16]. In the present study, we observed that CMKLR1 is upregulated by SHH/Gli pathway in MB. We found that chemerin/CMKLR1 signals via Gα(i)βγ and PI3K/Akt, and forms a complicated crosstalk with SHH pathway to collaboratively promote the development of MB.

MATERIALS AND METHODS

Small RNAs and gene overexpression constructs

Complementary strands of siRNAs were synthesized by GenePharma (Shanghai, China). Lentiviral vector containing the CMKLR1 overexpression cassette was obtained from Hanbio (Shanghai, China), and the shRNA-expressing lentiviral plasmid was obtained from (Genechem, Shanghai, China). For generation of recombinant lentiviruses, vectors were transfected into HEK293T cells along with packaging plasmids pMD2.G and psPAX2 (GeneChem). After transfection for 48 h, the supernatant was collected, centrifuged, filtered, and used for infection of target cells. The target sequences of siRNAs are listed in Table S1. To generate gene overexpression constructs, the cDNAs were amplified from total RNAs prepared from human whole blood cells, and cloned into a pGEM-T vector (Promega, Madison, WI), followed by subcloning into the appropriate sites of pcDNA3.1 (+) (Thermo Fisher, Waltham, MA). The primers for PCR amplification of cDNAs are listed in Table S1.

Cell culture, transfection and treatment

Human MB cell line ONS-76 was purchased from Qingqi Biotechnology Development Limited (Shanghai, China). Human MB cell line Daoy and human embryonic kidney 293 T (HEK293T) cells were purchased from National Infrastructure of Cell Line Resource (Beijing, China). Cells were cultured in Dulbecco's Modified Eagle Medium (DMEM; Sigma-Aldrich, Saint Louis, MO) supplemented with 10% fetal bovine serum (FBS; Biological Industries, Israel). Cells were routinely grown to 80% confluence at 37 °C in a humidified atmosphere containing 5% CO_2, and cells from passages 2–10 were used for experiments. Transfection was performed using Lipofectamine 2000 reagent (ThermoFisher Scientific-Invitrogen, Carlsbad, CA) or INTERFERin siRNA transfection reagent (Polyplus, Illkirch, France) according to the manufacturer's instruction. Where indicated, cells were treated with chemerin (Abcam, Cambridge, UK), a PI3K inhibitor (Ly294002, Selleck, Houston, TX), a PKA agonist (forskolin, Selleck), guanosine-5′-0-(3-thiotriphosphate) (GTPrs, NewEast Biosciences, King of Prussia, PA), a protein synthesis inhibitor (cycloheximide, Selleck) or a proteasome inhibitor (MG132, Selleck) at appropriate concentrations.

Transgenic mouse MB model

The spontaneous orthotopic MB model driven by Hedgehog signaling was from Jackson Laboratory (Bar Harbor, ME, stock #: 008831). These transgenic mice were developed on C57BL/6 strain and express SmoA1, a constitutively active mutant of the mouse homolog of the *Drosophila Smo* gene, under the control of the mouse neurogenic differentiation 2 (*Neurod2*) promoter, resulting in transgene expression specific to cerebellar granule cells [17]. Within the age of 20 to 30 weeks, mice develop tumor-related traits include enlarged posterior fossa, and/or tilted head, and hunched posture. Once clinical symptoms are noted, survival is normally 2 to 3 weeks.

RNA-sequencing and data analysis

Total RNA from paired control and Smo knockdown Daoy cells were prepared and subjected to RNA sequencing by Annoroad Gene Technology Corporation (Beijing, China). Briefly, mRNA was purified from total RNA using poly-T oligo-attached magnetic beads. The libraries were constructed and then paired-end sequencing with 150 bp reads was conducted on the Illumina platform (HiSeq, Illumina, San Diego, CA). After data cleaning, all clean reads were mapped to the reference genome (hg38) using Hisat2 v2.0.5. The gene expression level was measured by the fragments per kilobase per million (FPKM). Genes with $P < 0.05$ and $\log_2$Fold Change > 1 were considered differentially expressed genes (GEO: GSE147727).

Quantitative RT-PCR analysis

Total RNA was extracted using TRIzol reagent (Invitrogen) and reverse-transcribed to cDNA. cDNA was amplified by quantitative PCR using the SYBR Premix Ex Taq™ (Takara, Tokyo, Japan). The level of mRNAs was normalized to GAPDH, and the relative expression of genes was calculated with the $2^{-\triangle\triangle CT}$ method. The primers for PCR are listed in Table S1.

Western blotting

Cells were harvested at the indicated times, and total proteins were extracted for analysis. Protein concentrations were quantified using a BCA kit (Pierce, Waltham, MA). The proteins with loading buffer added were boiled for 10 min, except for cell membrane proteins such as G-protein and CMKLR1, which were mixed with loading buffer and left at room temperature for 30 min. Proteins were separated on SDS/PAGE gels, transferred onto PVDF membrane, and subjected to immunoblot analyses using the antibodies listed in Table S2. Horseradish peroxidase (HRP)–linked $F(ab)_2$ fragments of goat anti-rabbit and anti-mouse immunoglobulin (ZB-2305, Zhong Shan Jin Qiao, Beijing, China) were used as secondary antibodies.

Measurement of chemerin via ELISA

The concentration of chemerin in peripheral blood and tissues was measured by a commercial chemerin ELISA kit (ab204520, Abcam). In brief, antibody specific for chemerin was used to pre-coat a microplate. The serum or tissue lysate samples were prepared, and standards and samples were pipetted into the wells to allow antigen binding by the immobilized antibody. After removing any unbound substances, a biotin-conjugated antibody specific for chemerin was added to the wells. After washing, avidin-conjugated HPR was added to the wells, followed by a wash to remove any unbound avidin-enzyme reagent. The substrate solution was added to the wells for color development. The intensity of the color was measured, and the absolute protein levels were interpolated from the standard curve.

Molecular simulations and modeling

The structure of CMKLR1 (Uniport accession number: Q99788) was modeled using the I-TASSER approach (http://zhanglab.ccmb.med.umich.edu/I-TASSER), and evaluated by Profile-3D module and Procheck program [18, 19]. The coordinates of Gi heterotrimer protein consisting of Gα(i), Gβ and Gγ (PDB ID: 1GP2) were retrieved from RCSB Protein Data Bank (http://www.rcsb.org/pdb), and the missing residues Cys3, Thr4 and Lys349-Phe354 of Gα(i), and residues Arg62-Leu71 of Gγ were respectively modeled using the MODELER module, with the templates of green fluorescent protein (PDB ID: 3DQ8) and heterotrimeric G protein β1 and γ2 subunits (PDB ID: 1OMW) [18]. All the hetero-atoms were removed, and missing hydrogen atoms were added using Discovery Studio, based on the expected charge distributions of amino acids at neutral pH [18]. The two protein structures were geometry-optimized using the conjugate gradient (CG) method, and further refined by the 500 ns explicit solvent molecular dynamics (MD) simulations using GROMACS2018.8 and Charmm36m force field [20]. Protein-protein docking simulations were performed using the ZDOCK and RDOCK programs [21]. The optimal docked complex was selected on basis of energy and the size of cluster, and optimized using the conjugated gradient (CG) algorithm, with a convergence criterion of 0.01 kcal/mol. Each energy-minimized complex was further refined by the 1000 ns MD simulations. Structural plotting and visualization were accomplished by Discovery studio and UCSF Chimera [18, 22].

Co-immunoprecipitation (Co-IP)

The Co-IP assay was performed using the Immunoprecipitation kit (P2179S, Biyuntian Biotechnology, Shanghai, China) as per the manufacturer's instructions. Briefly, Daoy cells were lysed in lysis Buffer with protease inhibitor cocktail and centrifuged, and the supernatants were collected. Subsequently, 10 µg of anti-Gα(i) antibody (12617-1-AP, Proteintech, Wuhan, China), anti-Gα(o) antibody (GTX114439, GeneTex, Irvine, CA, USA), or control IgG was added to 25 µl of protein A/G magnetic beads. The mixture was incubated at room temperature for 1 h, followed by overnight incubation at 4 °C with cell lysates under constant rotation. The

beads were washed thrice with TBS, and the proteins were eluted using loading buffer for immunoblot analysis.

Luciferase reporter assay

For the promoter activity assay, a 2 kb fragment upstream of the transcription start site of *CMKLR1/RGS16* (wild-type and mutant) was cloned into the pGL4 vector (Promega, Madison, WI). The resultant constructs, together with a Renilla luciferase control vector (pGL4-RL, Promega) for normalization, and a Gli2-expresssing plasmid (pcDNA3.1-Gli2) were introduced into HEK293T cells. At 48 h post-transfection, cells were harvested and the Firefly and Renilla luciferase activities were measured using the Dual Luciferase Reporter Assay System (Yeasen Biotechnology, Shanghai, China).

Chromatin immunoprecipitation (ChIP)

Cells were cross-linked with formaldehyde and harvested for ChIP. Briefly, chromatin was fragmented by sonication, and pre-cleared chromatin was immunoprecipitated overnight with a Gli2 antibody (702013, ThermoFisher, Waltham, MA, USA) or IgG as a negative control. The enrichment of specific DNA fragments was analyzed by PCR. The primers used for amplification of human promoter regions are as follows: 5′-ATCAGACAGACTCAGATCCA-3′ and 5′-ACCAAGTGTGCCGAATGA-3′ for *CMKLR1*, 5′-CCTTATATGTTGTCACGGATG-3′ and 5′-AGAGGTCCTTAACGAGAAC-3′ for *RGS16*, and 5′-GGCAAATGCCTGACTCAGTGACC-3′ and 5′-TGACTCACCGTCCGGTCTCCCAGCA-3′ for *TUBB3* used as a negative control.

PKA activity assay

PepTag Assay for non-radioactive detection cAMP-dependent Protein Kinase (Enzo Life Sciences, Farmingdale, NY) was employed to measure the cellular activity of PKA following the manufacturer's protocol. All experiments were performed in triplicate.

Gα(i) activity assay

Gα(i) pull-down activation assay (NewEast Biosciences) was performed following the manufacturer's protocol. In brief, anti-Gα(i)-GTP antibody was incubated with cell lysates for 1 h, and then the GTP-bound Gα(i) was pulled down by protein A/G agarose. The activated Gα(i)-GTP was detected through Western blot analysis using an anti-Gα(i) antibody.

Protein stability and ubiquitination assays

For measurement of Gli2 stability, Daoy cells were transfected with control or CMKLR1/PRKACA-targeted siRNAs, followed by treatment of cells with forskolin and cycloheximide. Cells were then harvested at various time points for Western blot analysis. Alternatively, wild-type Gli2 (Gli2-WT) and a mutant at Ser234 (Gli2-S234A) were inserted into the pHAGE-IRES-ZsGreen lentivirus vector for overexpression. Daoy cells were first transfected with Gli2 siRNA to silence endogenous Gli2. Subsequently, the Gli2-WT or Gli2-S234A plasmid was transfected into the cells, followed by measurement of Gli2 stability as described above. For protein ubiquitination assay, cells were co-transfected with a construct for HA-tagged ubiquitin and siRNAs for 48 h, and treated with 10 μM proteasome inhibitor MG132 for 4 h. Cell lysates were immunoprecipitated with anti-Gli2 antibody (18773, Cell Signaling Technology, Boston, MA) and immunoblotted with anti-HA antibody.

Cell proliferation assay

Cell proliferation was measured using the Cell Counting Kit-8 (CCK-8; 7Sea Biotech, Shanghai, China). Briefly, harvested cells were seeded into 96-well plates at a density of 2000 cells/well ($n = 5$ for each time point) in a final volume of 100 μL. CCK-8 solution (10 μL) was added to each well, and the absorbance at 450 nm was measured after incubation for 2 h at 37 °C to calculate the number of viable cells.

Cell migration assay

For the wound-healing assay of cell migration, cells were seeded in a 24-well plate and incubate to reach confluence. The monolayer of cells was scratched using a tip and washed with PBS to remove detached cells. Then, the cells were cultured in serum-free medium for 0 h or 24 h and photographed. The migration rate was calculated as follows: migration Rate (%) = $(Area_{0h} - Area_{24h})/Area_{0h}$.

Immunofluorescent staining and images analysis

Cells were fixed with 4% paraformaldehyde for 20 min, followed by permeabilization with 0.5% Triton and blocking with 3% BSA. Cells were then incubated overnight at 4 °C with FITC-conjugated or unconjugated primary antibodies (Table S2). Cells were further stained with a Cy3-conjugated secondary antibody for 1 h in the dark at room temperature, and then incubated with 4′-6-diamidino-2-phenylindole (DAPI) for 8 min to stain the nuclei. Fluorescent images were captured by a laser confocal scanning microscopy.

Clinical specimens

Medulloblastoma samples were collected from patients receiving surgery in Department of Neurosurgery, Tangdu Hospital, Fourth Military Medical University. All patients have signed the written informed consent. Freshly cut 3-μm FFPE slides were prepared and immunohistochemistry analyses were performed. The samples were subject to GAB1 staining to distinguish SHH and other subgroups of MBs.

In vivo MB models and examinations

Athymic nude mice (6–8 weeks old) were injected subcutaneously with Daoy cells stably expressing *Renilla* luciferase together with scrambled or CMKLR1-/PRKACA-targeted shRNA (5×10^6 cells per mouse) to allow for xenograft tumor development. Bioluminescence was imaged on a Xenogen IVIS Kinetic imaging system (Caliper, Hopkinton, MA). Identical illumination settings (2/f stop, 12.5 cm field of view, binning factor of 4, open filter, 1 min exposure time) were used for all images. Tumor diameter was measured using a Vernier caliper every 7 days, and tumor size was estimated using the following formula: tumor volume = length × $width^2$ /2, where the length and width represented the longest and shortest tumor diameters, respectively. For study using the orthotopic MB model, Smo-transgenic mice received a weekly intraperitoneal injection of a chemerin antibody (4 ng/g, R&D Systems, Minneapolis, MN, Cat. #AF2325) or an isotypic control from postnatal day 28, and the survival of mice were monitored. Alternatively, mice were sacrificed at the age of 4 months, and the cerebella were isolated and weighed. To assess the impact of CMKLR1 and PRKACA knockdown on the survival of Smo-transgenic mice, shRNA-expressing recombinant adenoviruses (1×10^{12} PFU/ml, 2.5 μl) were used for intracerebellar injection of mice upon the onset of tumors indicated by observable symptoms like head tilt and altered gait. All intracranial injections were performed on adult mice under 2% isoflurane anesthesia. According to the stereotactic coordinates of the mouse brain (AP–4.5 mm, ML ± 1.5 mm, DV-3 mm), a sterile surgical procedure was carried out to expose the injection sites at these positions.

Histological staining

Mice were anesthetized with 10% chloral hydrate and perfused through the ascending aorta with 20 mL of normal saline (NS) (0–4 °C) followed by 20 mL of 4% paraformaldehyde (0–4 °C). The brain was removed, and the cerebellum was isolated, fixed in 10% formalin, and embedded in paraffin. Five-micron-thick sections were cut and subjected to immunohistochemical staining. H & E staining was conducted using a kit (Servicebio, G1076) according to the manufacturer's guidelines. Paraffin sections were deparaffinized, hydrated, and treated with pretreatment solution for 1 min. Subsequently, the sections were stained with hematoxylin solution for 5 min and eosin dye for 15 s. For immunohistochemistry (IHC) staining, antibodies listed in Table S2 were used. Chromogen development was performed with the ultraView Universal DAB detection kit (Ventana Medical Systems, Tucson, AZ). The percentage of positive cells and staining intensity were multiplied to produce a weighted score for each case.

Bioinformatics analysis

RNA-sequencing data were subject to the Gene Ontology (GO) enrichment analysis and Gene Set Enrichment Analysis (GSEA). Transcription factor binding sites on gene regulatory regions were predicted using the JASPAR online tool (http://jaspar.binf.ku.dk).

Public data analysis

Gene expression data were retrieved from MAGIC (Medulloblastoma Advanced Genomics International Consortium) cohort (GSE85217), which also contained clinical information of the 763 MB patients including 223 SHH-subtype MB cases. For survival analysis, Log-rank test was performed to assess the statistical significance of differences between groups.

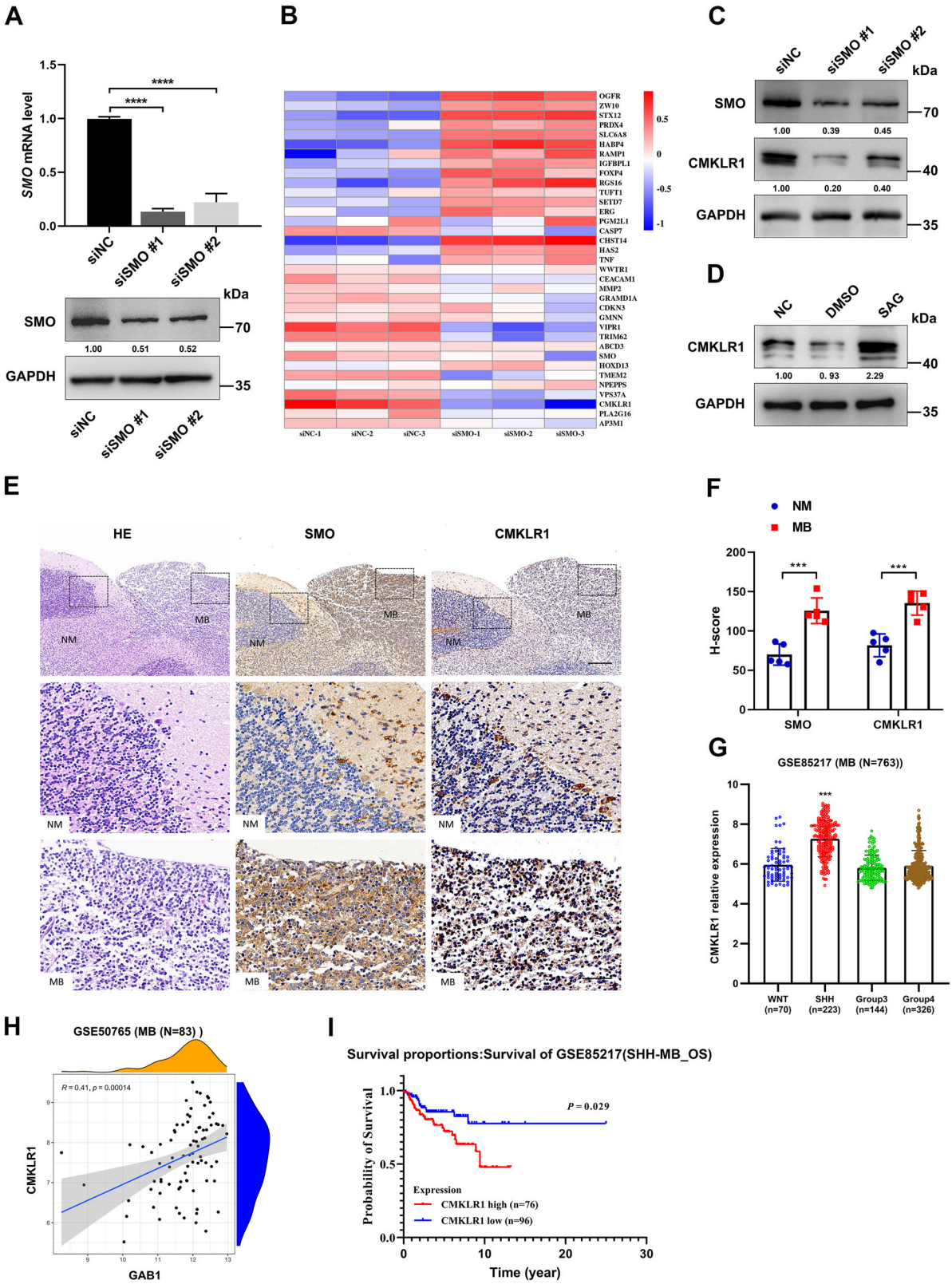

Significance analysis of CMKLR1 expression between subgroups was carried out by Kruskal-Wallis H test. Furthermore, gene expression profiles of 83 primary SHH-driven medulloblastoma samples (GSE50765) were acquired to investigate relationships between the expression of different genes within the cohort.

Statistical analysis

Data were analyzed using the SPSS software as follows: (1) For experiments including qRT-PCR, cell proliferation, cell migration, and luciferase assays, statistical significance was evaluated using the two-tailed Student's *t*-test for comparison of 2 groups, and ANOVA followed

Fig. 1 CMKLR1 is downregulated in SHH subgroup MB cells. A Human MB Daoy cells were transfected with indicated siRNAs, and were subject to qRT-PCR (upper panel) and Western blot (lower panel) analyses. **B** RNA-sequencing using paired control and Smo knockdown cells was performed and a heatmap of differentially expressed genes was shown. **C** Cells were transfected as described in (A), and were subjected to Western blot analyses. **D** Human MB ONS-76 cells were treated with a Smo agonist (SAG, 250 nM) for 48 h, and were subjected to Western blot analyses. **E**, **F** Representative images of H & E staining and immunohistochemical staining of Smo and CMKLR1 in the carcinoma and paracancerous tissue of SHH-MB samples from transgenic mice that spontaneously develop Smo-driven MB (Jackson Laboratory, Stock # 008831) (**E**). Statistical analysis of Histochemistry score (H-score) of Smo and CMKLR1 in SHH-MB samples (n = 5) was performed (**F**). NM, normal tissue. MB, medulloblastoma. Scale bar represents 200 μm in the upper panel and 50 μm in the middle and lower panel. **G**–**I** A Gene Expression Omnibus (GEO) dataset as indicated was used to analyze CMKLR1 expression (**G**), and the correlation of CMKLR1 and GAB1 levels (**H**) in all MB patients, and to perform Kaplan-Meier analysis for OS of SHH-subtype MB patients grouped by the expression level of CMKLR1 (**I**). Data are representative images or expressed as the means ± SD of three independent experiments. ***$P < 0.001$, ****$P < 0.0001$.

by Fisher's exact test for comparison of 3 or more groups. (2) For associations between gene expression values, significance was evaluated by Pearson product–moment correlation coefficient analysis.

RESULTS

Aberrant chemerin/CMKLR1 signaling in SHH-subtype MB

We previously investigated the gene profiles in an orthotopic MB model driven by the constitutively active form of Smoothened (Smo, Jackson Laboratory, Stock # 008831) [17], the serpentine receptor of Hedgehog pathway, and identified aberrantly expressed genes by comparing them with genes expressed in normal CGNPs (data deposited in GEO, assigned accession # GSE85449) [23]. To further screen for genes that mediate MB development downstream of SHH signaling, we silenced Smo in a documented SHH-driven MB cell line, Daoy [24], and performed RNA-seq analysis (data deposited in GEO, assigned accession # GSE147727) (Fig. 1A, B). We thus selected differentially expressed genes (DEGs) that were overlapped in the above gene profiling assays for qRT-PCR validation (Fig. S1A), and found that the mRNA level of chemerin receptor, CMKLR1, exhibited the most dramatic decrease after knockdown of Smo in Daoy cells (Fig. S1B). Consistently, Smo knockdown significantly reduced the protein level of CMKLR1 in Daoy cells (Fig. 1C). We next treated ONS-76, another SHH subtype human MB cell line expressing a moderate level of Smo [24], with a Smo agonist (SAG), and detected a remarkable upregulation of CMKLR1 (Fig. 1D). In addition, CMKLR1 was highly expressed in tumor tissues compared with adjacent normal cerebellar tissues in the above-mentioned mouse orthotopic MB model (Fig. 1E, F). In parallel, we observed a significant increase in the levels of chemerin both in mouse MB compared with the paracancerous tissues and in the serum of MB-bearing mice compared with their healthy littermates (Figs. S2A, B). Data analysis using public GEO datasets of MB revealed high expression of CMKLR1 specifically in the SHH-subtype MB (Fig. 1G), and a correlation between the levels of CMKLR1 and GAB1, a documented biomarker of SHH subgroup MB (Fig. 1H) [25]. Furthermore, SHH-subtype MB patients with higher CMKLR1 expression showed poorer overall survival (OS) rates than those with low CMKLR1 expression (Fig. 1I). Thus, chemerin/CMKLR1 signaling is potentially involved in the pathogenesis of SHH-subtype MB.

Chemerin/CMKLR1 promotes malignant phenotypes of MB cells via PI3K/Akt signaling

We next investigated whether CMKLR1 plays a regulatory role in the malignant behaviors of MB. We found that knockdown of CMKLR1 in Daoy cells significantly repressed the growth or proliferation of MB cells (Fig. 2A, B), whereas its overexpression in ONS-76 cells, which express a relatively low level of endogenous CMKLR1, improved the growth of these cells (Fig. 2C, D and Fig. S3A). In accordance with these observations, we found that incubation of Daoy cells with chemerin resulted in enhanced cell growth (Fig. S3B). CMKLR1 knockdown and ectopic expression also attenuated and enhanced the migration capacity of MB cells, respectively (Fig. 2E, F). Consistently, chemerin treatment increased the migration capability of Daoy cells (Fig. S3C). However, it is likely that serum but not autocrine chemerin represents the major source of the CMKLR1 ligand since knockdown of chemerin failed to significantly affect the growth of MB cells (Fig. S4A, B). Of the downstream pathways potentially affected by chemokine signaling, we found that treatment of Daoy cells with Chemerin or overexpression of CMKLR1 in ONS-76 cells led to enhanced Akt phosphorylation (Fig. 2G, H). Conversely, knockdown of CMKLR1 in Daoy cells resulted in a decrease in Akt phosphorylation (Fig. 2H). In addition, while chemerin treatment promoted the malignant phenotypes of MB cells, this was ablated by the inhibition of PI3K/Akt signaling (Fig. 2I, J). Therefore, chemerin/CMKLR1 signaling potentiates the growth and migration of MB cells via PI3K/Akt pathway.

CMKLR1 activates PI3K/Akt pathway through Gi-mediated signaling

CMKLR1 is a G protein-coupled receptor reported to associate mainly with Gi/o subtype G proteins [11]. We thus explored how CMKLR1 signals to activate the PI3K/Akt pathway. We found that knockdown of the α(i) subunit or the constitutive β subunit of G proteins, but not the α(o) subunit, abrogated the activation of Akt (Fig. 3A). Consistently, CMKLR1 binding to Gi was supported by a modeling study based on published protein crystal structures (Fig. 3B), and Gi colocalization with CMKLR1 on the cytomembrane of MB cells was validated by immunofluorescence staining (Fig. 3C). Immunoprecipitation assay validated the association of CMKLR1 with Gα(i) but not Gα(o) in Daoy cells in the presence of chemerin (Fig. 3D). In addition, we verified that Gα(i) and Akt were activated after incubation with chemerin, which was hindered by the knockdown of CMKLR1 in Daoy cells (Fig. 3E) and enhanced by the overexpression of CMKLR1 in ONS-76 cells (Fig. 3F). Similar to knockdown of CMKLR1, silencing of the α(i) subunit also led to suppressed growth and migration of MB cells (Fig. 3G, H). These data suggest that CMKLR1 promotes MB pathogenesis through Gi/PI3K/Akt signaling.

The hedgehog receptor SMO maintains CMKLR1/Gi signaling via transcriptional regulation of CMKLR1 and RGS16

We next asked how SHH pathway regulated CMKLR1 and downstream signaling in MB cells. We found that knockdown of Gli2 but not other members of the Gli family transcription factors suppressed CMKLR1 expression in MB cells (Fig. S5A–C). Consistently, bioinformatics analysis of the *CMKLR1* promoter region revealed the existence of potential Gli2-binding elements (Fig. 4A). Indeed, a luciferase reporter assay indicated that the 5′ region containing these sites was responsible for Gli2 regulation of CMKLR1 (Fig. 4B), which was validated by ChIP assay showing the enrichment of Gli2 on *CMKLR1* promoter (Fig. 4C and Fig. S6A, B). In addition, the aforementioned RNA-seq data unraveled that the gene encoding Regulator of G Protein Signaling 16 (RGS16), a member of the negative G protein regulator family [26], was downregulated by SHH pathway (Fig. 1B). In line with these data, we observed that both luciferase reporter and ChIP assays verified

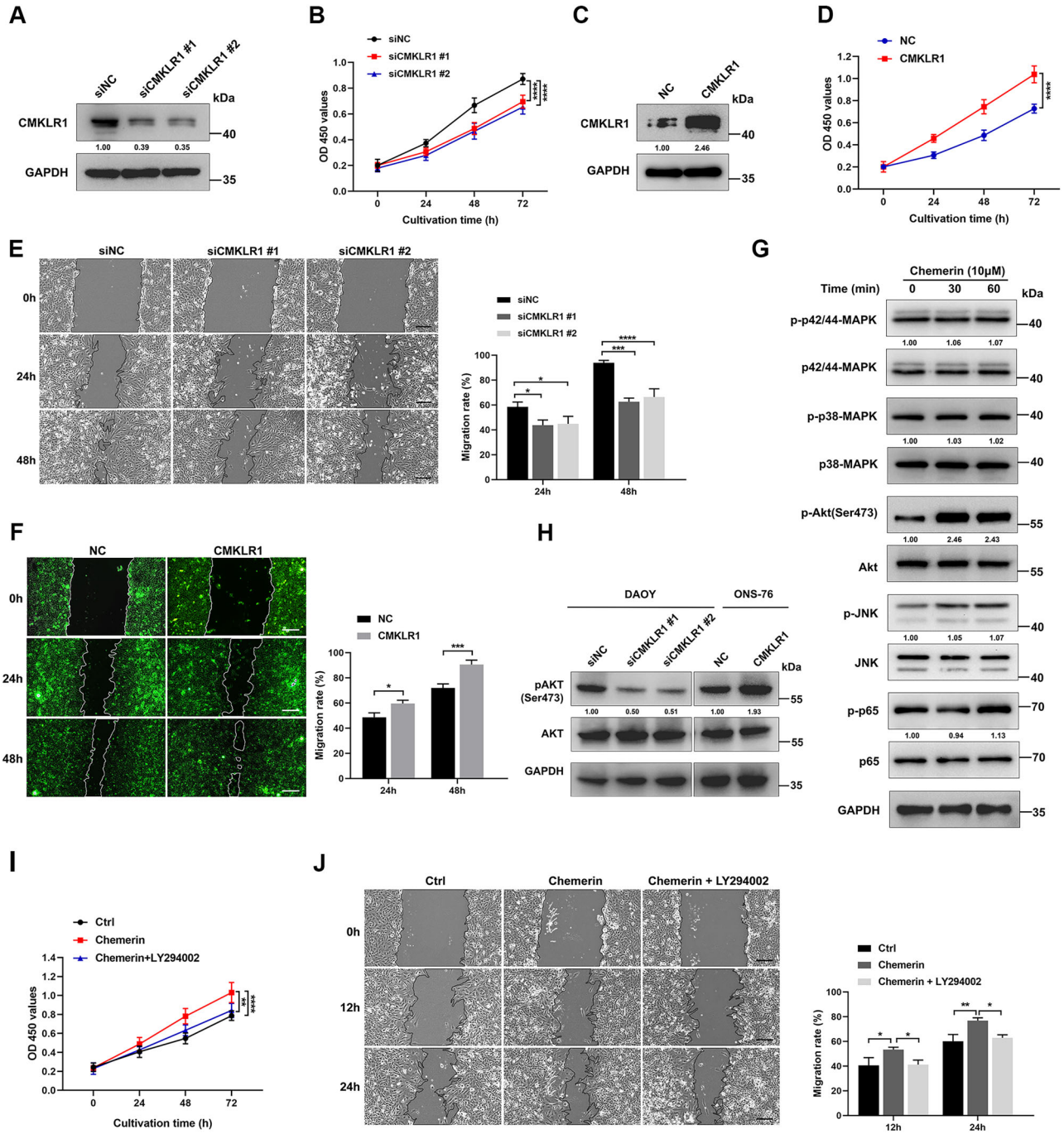

Fig. 2 CMKLR1 promotes MB cell growth and migration via PI3K/Akt pathway. A Daoy cells were transfected with indicated siRNAs and were subject to Western blot analyses. **B** Cells were transfected as described in (**A**), and were subjected to CCK-8 assay. **C** ONS-76 cells were infected with control or CMKLR1-overexpressing recombinant lentiviruses, and were subjected to Western blot analyses. **D** Cells were infected as described in (**C**), and were subjected to CCK-8 assay. **E, F** Daoy cells were transfected with indicated siRNA (**E**), and ONS-76 cells were infected with indicated recombinant lentiviruses (**F**). Cells were then subjected to wound-healing assay for migration. **G** Daoy cells were treated with chemerin (10 μM) and were subjected to Western blot analyses. **H** Cells were transfected as described in (**E** and **F**), and were subjected to Western blot analyses. **I, J** Daoy cells were treated with chemerin (10 μM) and Ly294002 (100 μM) as indicated. Cells were then used for CCK-8 (**I**) and wound-healing (**J**) assays. Bar, 200 μm. Data are representative images or expressed as the means ± SD of three independent experiments. *$P < 0.05$, **$P < 0.01$, ***$P < 0.001$, ****$P < 0.0001$.

the transcriptional repression of *RGS16* by Gli2 (Fig. 4D–F). Consistently, we observed that Smo silencing in MB cells downregulated the transcription factor Gli2 and promoted *RGS16* expression with concomitantly reduced Gα(i) and Akt activation (Fig. 4G, H). Overexpression of RGS16 in Daoy or ONS-76 cells impaired chemerin-induced activation of Gα(i) and the phosphorylation of Akt (Fig. 4I). In Smo knockdown MB cells, further silencing of RGS16 at least partially restored Gα(i) activation and Akt phosphorylation (Fig. 4J). Data analysis using the aforementioned GEO dataset (accession # GSE50765) validated the reverse correlation of RGS16 levels with that of GAB1 or CMKLR1 (Fig. 4K, L). Thus, SHH licenses *CMKLR1* expression while

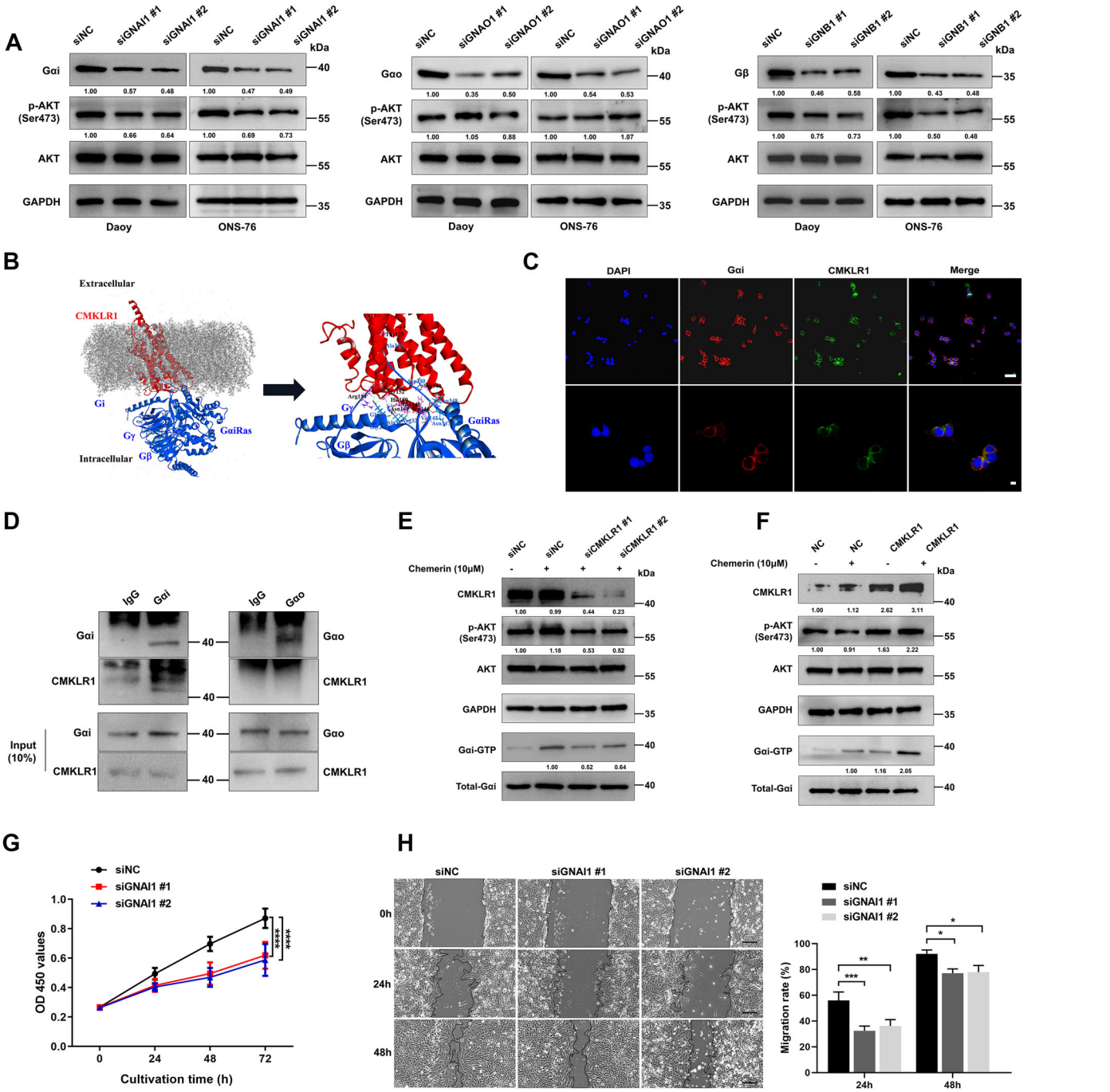

Fig. 3 CMKLR1 activates PI3K/Akt pathway through α(i) subunit-containing G protein. A Daoy cells and ONS-76 cells were transfected with indicated siRNAs, and were subjected to Western blot analyses. GNAI1, GNAO1 and GNBI1 are genes encoding the α(i), α(o) and β subunits of human G protein, respectively. **B** Propeller structure and key residues within the binding interface of CMKLR1-Gi complex. The key residues of CMKLR1 and Gi are represented by stick models. The C atoms are colored in pink and powder blue for CMKLR1 and Gi, and the N and O atoms are colored in blue and red, respectively. H-bonding interactions are labeled in dashed green lines. **C** Daoy cells were used for immunofluorescence staining with the indicated antibodies and were subjected to confocal microscopy. Bar, 50 μm (upper panel) and 10 μm (lower panel). **D** Daoy cells were treated with chemerin (10 μM), and the cell lysates were prepared and subjected to immunoprecipitation assays. **E**, **F** Daoy cells were transfected with the indicated siRNAs and/or treated with chemerin (**E**) and ONS-76 cells were infected with indicated recombinant lentiviruses and/or treated with chemerin (**F**). Cell lysates were then prepared for Western blot and Gα(i) activity assays. For Gα(i) activity assay, lysates were subjected to pull-down of GTP-bound Gα(i) and subsequent Western blot using an anti-Gα(i) antibody. **G**, **H** Daoy cells were transfected with the indicated siRNAs and were subjected to CCK-8 assay for cell growth (**G**) or wound-healing assay for cell migration (**H**). Bar, 200 μm. Data are representative images or expressed as the means ± SD of three independent experiments. $^{*}P < 0.05$, $^{**}P < 0.01$, $^{***}P < 0.001$, $^{****}P < 0.0001$.

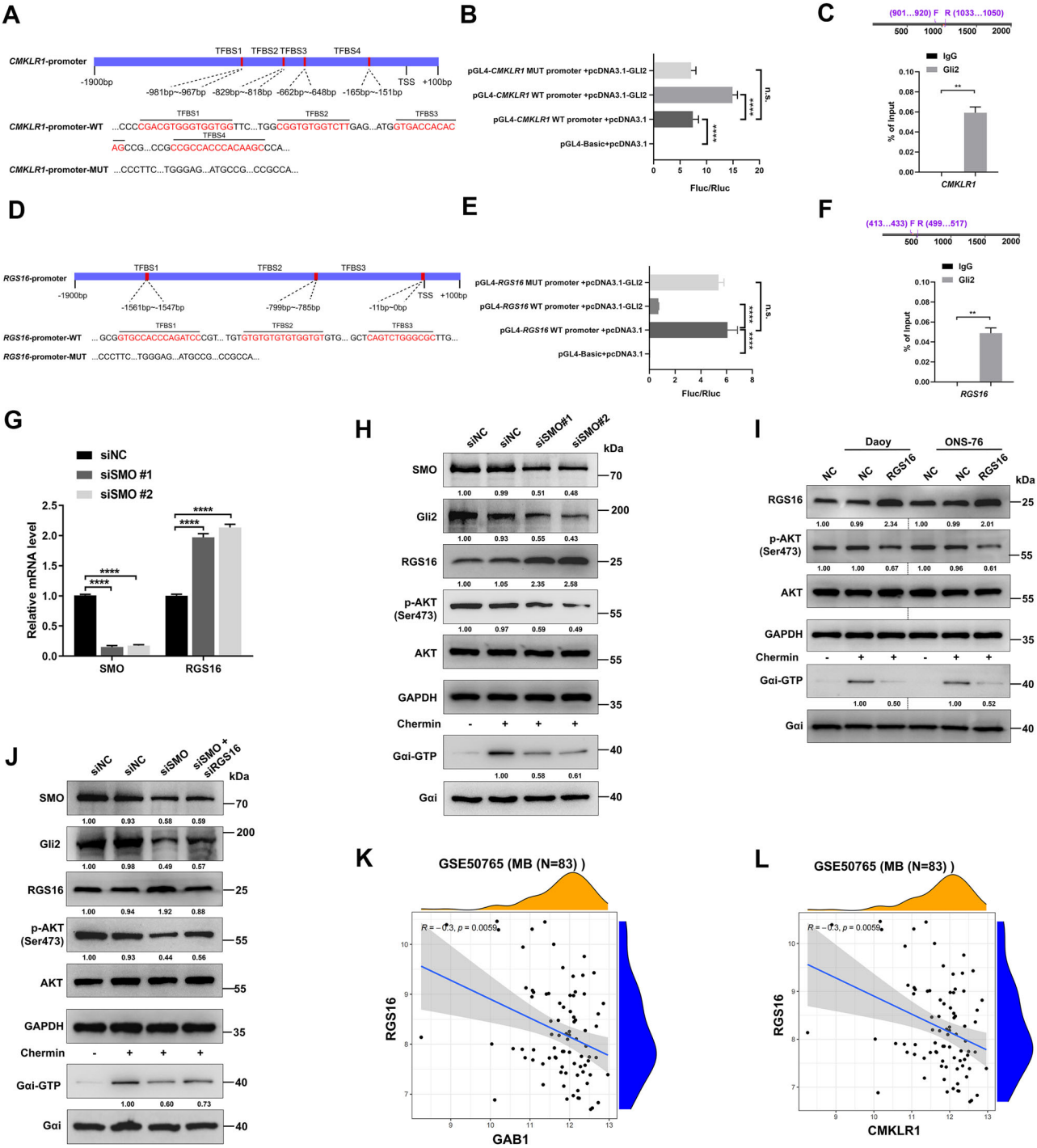

Fig. 4 SHH signaling dictates the expression of CMKLR1 and RGS16. A–**F** The potential Gli2 binding sites on *CMKLR1*/*RGS16* promoter regions were predicted (**A**, **D**). The pGL4 constructs for wild-type (wt) or the predicted Gli2 binding sites-mutated (mut) *CMKLR1*/*RGS16* promoter sequences were generated, and were used for co-transfection of HEK293T cells with a Gli2-overexpressing plasmid, followed by measurement of luciferase activity in the transfected cells (**B**, **E**). ChIP-PCR assay was performed using Daoy cells to detect the enrichment of Gli2 on *CMKLR1*/*RGS16* promoter, and Immunoglobulin G (IgG) were included as a control (**C**, **F**). TFBS, transcription factor binding site. **G**, **H** Daoy cells were transfected with indicated siRNAs, and were subjected to qRT-PCR (**G**), Western blot and Gα(i) activity assays as described in Figs. 3E and 3F (**H**). **I**. Daoy and ONS-76 cells were transfected with a control or RGS16-overexpressing construct, and cultured in media supplemented with or without chemerin. Cell lysates were then prepared for Western blot analyses of the indicated proteins or for Gα(i) activity assay. **J** Daoy cells were transfected with indicated siRNAs, and were subjected to Western blot and Gα(i) activity assays. **K**, **L** Statistical analysis for the correlation of RGS16 with GAB1 (**K**) or CMKLR1 (**L**) using the indicated GEO dataset. Data are representative images or expressed as the means ± SD of three independent experiments. $^{**}P < 0.01$, $^{****}P < 0.0001$, n.s., non-significant.

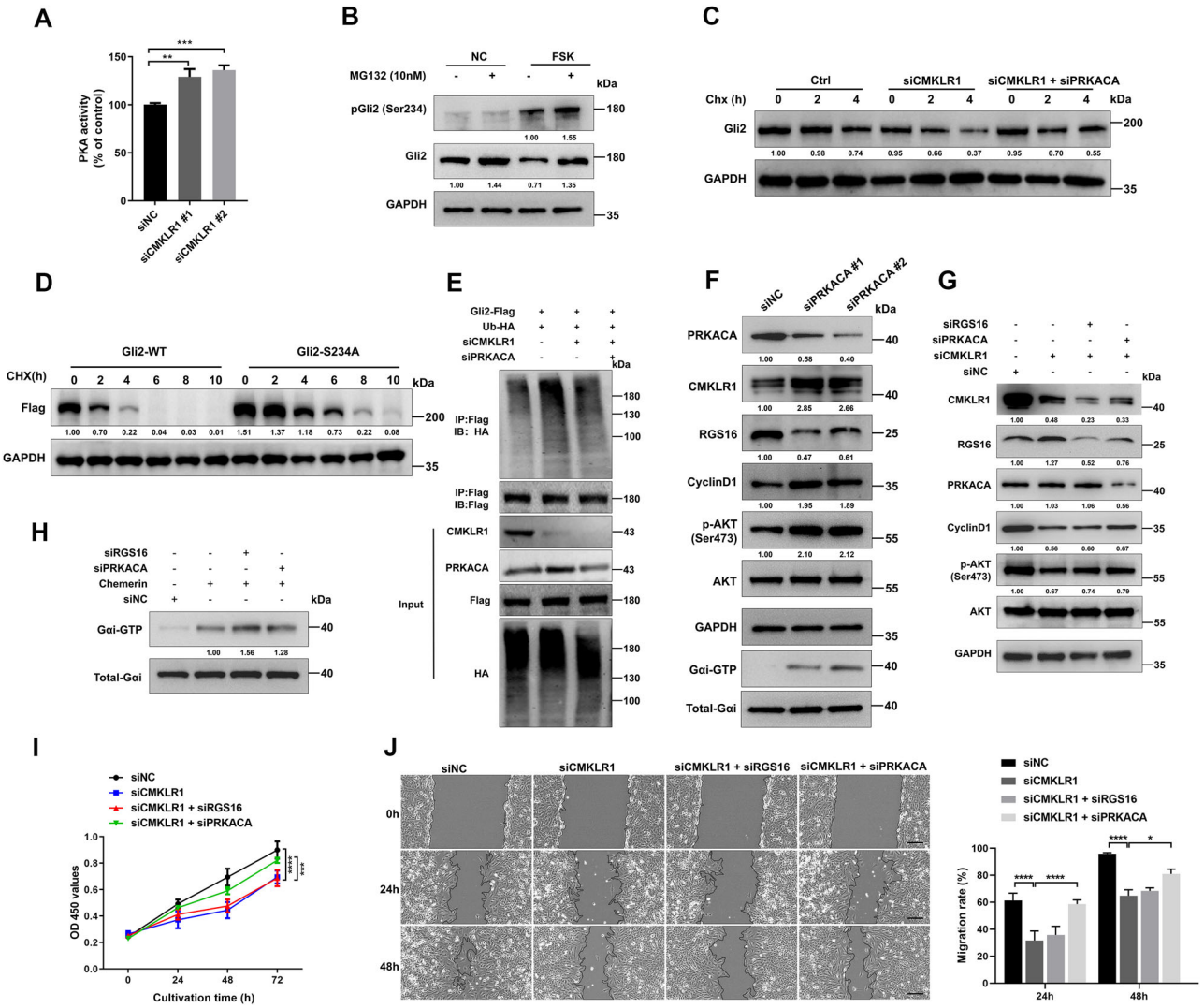

Fig. 5 CMKLR1/Gi reinforces SHH signaling through repression of PKA. A Daoy cells were transfected with indicated siRNAs and subjected to measurement of cellular PKA activity. **B** Daoy cells were treated with or without MG132 (10 μM) and/or Forskolin (FSK, 50 μM) for 12 h, and were subjected to Western blot analysis. **C** Daoy cells were transfected with indicated siRNAs, and treated with cycloheximide (CHX, 20 μM) for indicated times. Cell lysates were then prepared for Western blot analysis. **D** Daoy cells were subjected to knockdown of endogenous Gli2 by siRNA, followed by transfection with the construct of wild-type Gli2 or an S234A mutant. Cells were then treated with FSK (50 μM) and CHX (20 μM), and the lysates were then used for Western blot analyses. **E** Daoy cells were transfected with the indicated siRNAs and/or constructs for HA-tagged Ubiquitin and Flag-conjugated Gli2 in the presence of MG132. Cell lysates were then prepared and subjected to immunoprecipitation and Western blot analyses. **F**, **G** Daoy cells were transfected with indicated siRNAs, and were subjected to Western blot analysis. **H** ONS-76 cells were incubated with Chemerin and the indicated siRNAs, followed by Gα(i) activity assay. **I**, **J** Daoy cells were transfected with indicated siRNAs, and were subjected to CCK-8 assay for cell growth (**I**) or wound-healing assay for cell migration (**J**). Bar, 200 μm. Data are representative images or expressed as the means ± SD of three independent experiments. $^{*}P < 0.05$, $^{**}P < 0.01$, $^{***}P < 0.001$, $^{****}P < 0.0001$.

transcriptionally repressing *RGS16*, which coordinately activates CMKLR1/Gi signaling in MB cells.

CMKLR1/Gi signaling reinforces SHH pathways through PKA repression

Gi proteins play inhibitory roles in the activation of protein kinase A (PKA), while PKA was reported to phosphorylate and elicit the proteasomal degradation of Gli transcription factors [4, 27]. We thus inferred that CMKLR1 might exert a feedback regulation on SHH signaling via PKA repression. Indeed, we found that CMKLR1 knockdown promoted PKA activation in MB cells (Fig. 5A). Treatment of cells with the PKA agonist, Forskolin, enhanced the phosphorylation of Gli2 while reducing total Gli2 levels in the absence of MG132, a proteasomal protein degradation inhibitor, suggesting that PKA promotes phosphorylation-dependent Gli2 degradation (Fig. 5B). In line with these observations, we found that CMKLR1 knockdown expedited the degradation of Gli2, which was counteracted by further knockdown of the catalytic subunit of PKA (PRKACA, Fig. 5C). An introduction of mutation at the 234th serine of Gli2 remarkably counteracted PKA-triggered protein degradation in Daoy cells (Fig. 5D). CMKLR1 deficiency facilitated ubiquitination of Gli2, which was ameliorated by further silencing of PRKACA (Fig. 5E). In addition, depletion of PRKACA was verified to reinforce SHH signaling as evidenced by increased expression of a documented Gli target, cyclin D1 [28] (Fig. 5F). Concomitantly, PRKACA knockdown resulted in significant upregulation of *CMKLR1*, downregulation of *RGS16*, and increased activation of Akt and Gα(i) (Fig. 5F). However, in Daoy cells depleted of CMKLR1, further knockdown of PRKACA or RGS16 failed to improve Akt phosphorylation, although PRKACA but not RGS16 knockdown

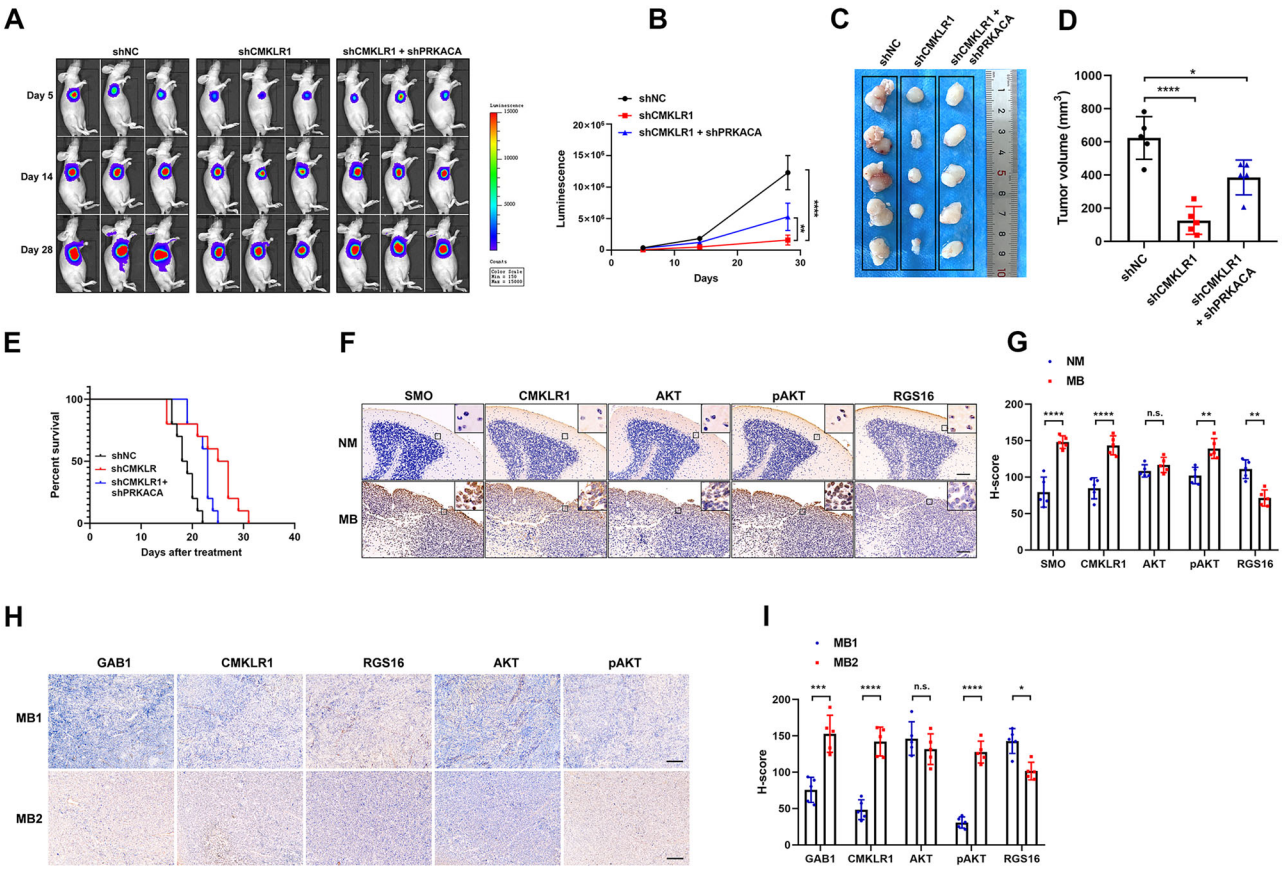

Fig. 6 Crosstalk between SHH and CMKLR1 pathways underlies in vivo development of MB. A–D Daoy cells were modified to express luciferase and further infected with lentiviruses expressing control, CMKLR1- or PRKACA-targeted shRNAs. Cells were then used for s.c. injection of male nude mice ($n = 5$). The development of xenograft tumors was visualized on indicated days via bioluminescence imaging (**A**), and the tumor bioluminescence signals in mice were recorded to follow tumor progression (**B**). On day 28 post-inoculation, mice were sacrificed, tumors were isolated (**C**) and the tumor volume was quantified (**D**). **E** Smo-transgenic mice received intracerebellar injection with shRNA-expressing recombinant adenoviruses (1×10^{12} PFU/ml, 2.5 μl) upon onset of tumors. The survival of mice were recorded daily for preparation of a Kaplan–Meier curve (n = 10). $P = 0.0029$ (shNC v.s. shCMKLR1) and $P = 0.0365$ (shCMKLR1 v.s. shCMKLR1+shPRKACA). **F, G** Tumors were isolated from transgenic mice that spontaneously develop Smo-driven MB (lower panel, $n = 5$), and normal cerebella were isolated from age-matched wild-type mice (upper panel, $n = 5$). The specimens were sectioned and subject to IHC staining for indicated proteins (**F**) and quantification of the staining results by H-score (**G**). NM, normal tissue. Bar, 100μm. **H, I** Representative images for immunohistochemical assays of clinical non-SHH (upper panel, $n = 5$) and SHH (lower panel, $n = 5$) MB samples (**H**). SHH subtype MB was distinguished by positive staining for GAB1 in IHC, and quantification of the staining results by H-score (**I**). Bar, 100μm. $^{*}P < 0.05$, $^{**}P < 0.01$, $^{***}P < 0.001$, $^{****}P < 0.0001$, n.s., non-significant.

was effective in upregulating cyclin D1 (Fig. 5G). In ONS-76 cells treated with chemerin, silencing of either RGS16 or PRKACA further enhanced the activation of Gα(i) (Fig. 5H). Finally, CMKLR1 ablation-elicited suppression of MB cell growth and migration was rescued by knockdown of PRKACA (Fig. 5I, J). Together, these findings indicate that CMKLR1/Gi promotes Hedgehog signaling through inactivation of PKA, thereby forming a regulatory circuit in the development of SHH-subtype MB.

Interplay between SHH and CMKLR1 pathways contributes to in vivo MB progression

We finally explored whether the CMKLR1/Gi signaling underlies the development and progression of SHH-driven MB in vivo. While all groups of cells including parental Daoy cells and those subjected to CMKLR1 and PRKACA knockdown formed xenograft tumors, silencing of CMKLR1 suppressed tumor growth in nude mice, which was partially restored by further knockdown of PRKACA (Fig. 6A–D). Consistently, CMKLR1 knockdown in Smo-driven MB significantly prolonged the survival of mice, an effect constrained by concomitant depletion of PRKACA (Fig. 6E). We then used the Smo-transgenic mice to evaluate the role of the aforementioned pathway in SHH-driven MB pathogenesis. As a result, we detected elevated expression of CMKLR1, reduced RGS16 levels and high phosphorylation of Akt when compared with the normal cerebellar tissues (Fig. 6F, G). In line with these findings, we found that treatment of these mice through intraperitoneal administration of a chemerin antibody significantly reduced cerebellar weight and prolonged survival of mice (Fig. S7A, B). Finally, staining of SHH-subtype clinical MB specimens revealed the upregulation of CMKLR1, the decrease in RGS16 levels and enhanced Akt phosphorylation compared with non-SHH MB specimens (Fig. 6H, I). These data demonstrate that the crosstalk between SHH and CMKLR1 pathways accounts for the in vivo occurrence and progression of MB.

DISCUSSION

The hyperactivation of Hedgehog pathway has been well documented to propel the occurrence and progression of various cancers [5, 6]. While poorly active in most adult organisms, it can be aroused as a result of somatic mutations in genes coding the elements of Hedgehog signaling, e.g. *Ptch1*, *Smo* and *Sufu*, and

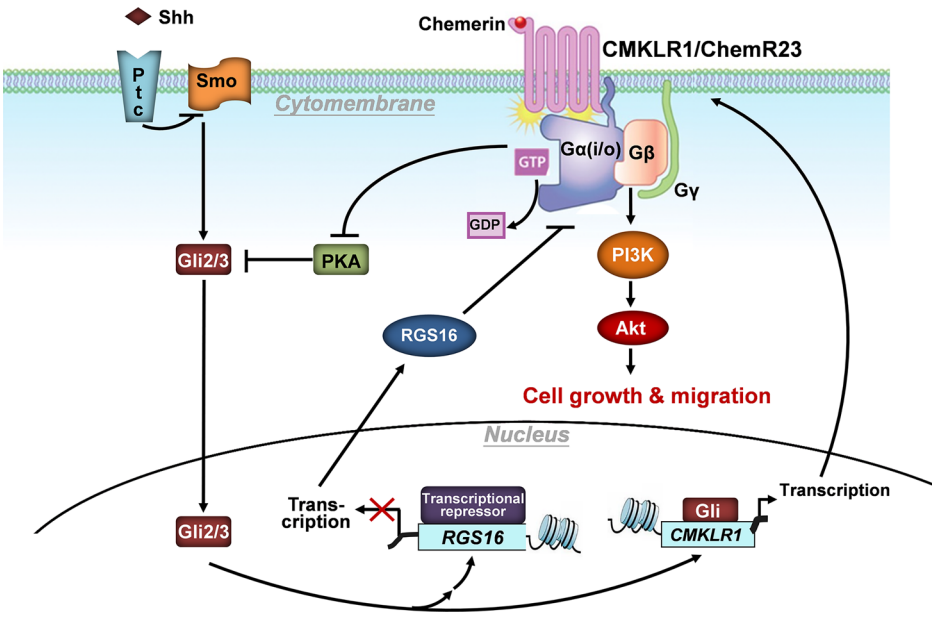

Fig. 7 A working model for crosstalk between SHH and CMKLR1 pathways in MB pathogenesis. The Sonic Hedgehog pathway triggers chemerin/CMKLR1 signaling through transcriptional activation of *CMKLR1* and repression of *RGS16*. Chemerin/CMKLR1 promotes the malignant behaviors of MB cells via Gi and PI3K/Akt pathway. Meanwhile, the activated Gi further expedites Hedgehog signaling through repression of PKA and thereby reduced phosphorylation of Gli2. Thus, the SHH/Gli and CMKLR1 pathways form a regulatory circuit to collaboratively orchestrate MB development.

thereby causes improved cell survival, proliferation and migration on cells, culminating in malignancies of different tissues [10, 29]. Despite a growing list of genes identified as transcriptional targets of Hedgehog pathway, those that drive malignant transformation may vary dependent upon the signaling context of individual cancer-initiating cells [30–33]. We established here that chemerin/CMKLR1 is a key mediator of SHH signaling that drives MB. While representative targets of Hedgehog pathway are players in cell differentiation and self-control of the signal strength, CMKLR1 might also provide a link between SHH/Gli pathway and canonical survival and pro-mitotic signal events, allowing for a deviation from balanced cell number growth and fate commitment [34]. Moreover, CMKLR1/Gi intensifies SHH signaling through impairing PKA-catalyzed phosphorylation and degradation of Gli2 in MB cells. These findings suggest a complicated reciprocal regulation between chemerin/CMKLR1 and SHH pathways, thus adding weight to their synergistical roles in the pathogenesis of MB (Fig. 7).

Histology alone has provided inadequate information required for identification of MBs of different origins, highlighting the importance of molecular subtyping based mainly on driver mutations and genetic landscapes of malignant cells [35, 36]. An integrated clustering of primary MB, while recovering the four classical subtypes, identified several clinically and cytogenetically distinct groups within SHH subtype MB, of which the SHHα group has the worst prognosis and is enriched for *MYCN* and *Yap1* amplifications [37]. Another genomic profiling study revealed that $OLIG2^{+}$ progenitors, the potential tumor-initiating population for SHH MB, exhibited activated oncogenic networks including Hippo-Yap/Taz and Aurora-A/N-Myc pathways [38]. In agreement with these findings, we demonstrated previously a crosstalk between SHH and Hippo/Yap1 pathways involving a long non-coding RNA in MB cells [23]. In the present study, we found that SHH/Gli promotes CMKLR1 signaling to inactivate PKA, a known repressor of Yap1 nuclear accumulation through phosphorylation of large tumor suppressor kinase 1/2 (LATS1/2) [39]. Further investigations are needed to probe whether the interplay between SHH and CMKLR1 pathways demonstrated by the present study occurs specifically in SHHα group MB featured by Yap1 overexpression. In addition, our in vitro observations were limited to MB cells with *SMO* mutation or subjected to silencing of SMO, and it is worth probing whether CMKLR1 and downstream signaling play a similar role in SHH subtype MB with *PTCH1* or *SUFU* mutation [5]. Finally, SHH subgroup MB displayed high expression of the core genes involved in TP53, AURORA and Polo-like kinase 1 (PLK1) pathways, whereas PKA was a reported negative regulator of PLK1 [40, 41]. Therefore, our findings together with mounting evidence from recent reports suggest the pivotal role of CMKLR1/PKA in cellular signaling events orchestrating the transformation of cerebellar granule neuron progenitors and in stratified classification of SHH-driven MB.

Chemerin is a pleiotropic protein critically involved in adipogenesis, inflammation, and glucose homeostasis [16, 42]. The diversity of chemerin isoforms due to C-terminal variations reflects the multiplicity of its biological roles [42, 43]. Literatures have revealed both anti-tumoral and tumor-promoting effects of this adipokine in various malignancies, which is dependent largely upon the responsive cells that express the chemerin receptor CMKLR1/Chem23 [13, 44]. Data presented by other researchers suggest that chemerin is tumor-suppressive when exerting a role on the subsets of cells involved in innate immunity [13, 44]. However, high level of circulating chemerin is strongly associated with cancer risk, and increased CMKLR1 expression in neoplastic cells was established to promote progression of most cancer entities including esophageal squamous cell carcinoma (ESCC), neuroblastoma, hepatocellular carcinoma and gastric cancer [15, 44, 45]. Likewise, we demonstrated in MB that chemerin/CMKLR1 signaling is activated by the Hedgehog pathway through distinct transcriptional regulation of *CMKLR1* and *RGS16*, a repressor of G protein signaling, and contributes to carcinogenesis via Gα(i)βγ and PI3K/Akt pathway [26]. Thus, these data suggest the applicability of blood-brain barrier-penetrating CMKLR1-binding peptides in tracing intracranial tumors like MB [46]. In addition, since GPCRs represent the leading family of validated drug targets in biomedicine, CMKLR1 inhibitors or antagonizing peptides are potentially applicable in the suppression of SHH-

driven MB [47]. Finally, given that a variety of small molecule inhibitors targeting the Hedgehog signaling, e.g. Smoothened inhibitors like vismodegib, have been developed or even approved for clinical use, our findings also provide a rationale for combined CMKLR1 and SHH pathway inhibition in the treatment of SHH-subtype MB [48].

DATA AVAILABILITY

The RNA sequencing data have been deposited at the GEO archive of NCBI (identifiers GSE147727 and GSE85449).

REFERENCES

1. Zhang Y, Beachy PA. Cellular and molecular mechanisms of Hedgehog signalling. Nat Rev Mol Cell Biol. 2023;24:668–87.
2. Petrov K, Wierbowski BM, Salic A. Sending and receiving Hedgehog signals. Annu Rev Cell Dev Biol. 2017;33:145–68.
3. Liu A. Proteostasis in the Hedgehog signaling pathway. Semin Cell Dev Biol. 2019;93:153–63.
4. Niewiadomski P, Kong JH, Ahrends R, Ma Y, Humke EW, Khan S, et al. Gli protein activity is controlled by multisite phosphorylation in vertebrate Hedgehog signaling. Cell Rep. 2014;6:168–81.
5. Wang W, Shiraishi R, Kawauchi D. Sonic Hedgehog signaling in cerebellar development and cancer. Front Cell Dev Biol. 2022;10:864035.
6. Jing J, Wu Z, Wang J, Luo G, Lin H, Fan Y, et al. Hedgehog signaling in tissue homeostasis, cancers, and targeted therapies. Signal Transduct Target Ther. 2023;8:315.
7. Orr BA. Pathology, diagnostics, and classification of MB. Brain Pathol. 2020;30:664–78.
8. Sheng H, Li H, Zeng H, Zhang B, Lu Y, Liu X. et al. Heterogeneity and tumoral origin of medulloblastoma in the single-cell era. Oncogene. 2024;43:839–50.
9. Wang J, Garancher A, Ramaswamy V, Wechsler-Reya RJ. MB: from molecular subgroups to molecular targeted therapies. Annu Rev Neurosci. 2018;41:207–32.
10. Haldipur P, Millen KJ, Aldinger KA. Human cerebellar development and transcriptomics: implications for neurodevelopmental disorders. Annu Rev Neurosci. 2022;45:515–31.
11. Zdanowicz K, Bobrus-Chociej A, Lebensztejn DM. Chemerin as potential biomarker in pediatric diseases: a PRISMA-compliant study. Biomedicines. 2022;10:591.
12. Yoshimura T, Oppenheim JJ. Chemokine-like receptor 1 (CMKLR1) and chemokine (C-C motif) receptor-like 2 (CCRL2); two multifunctional receptors with unusual properties. Exp Cell Res. 2011;317:674–84.
13. Goralski KB, Jackson AE, McKeown BT, Sinal CJ. More than an adipokine: The complex roles of chemerin signaling in cancer. Int J Mol Sci. 2019;20:4778.
14. Shin WJ, Zabel BA, Pachynski RK. Mechanisms and functions of chemerin in cancer: potential roles in therapeutic intervention. Front Immunol. 2018;9:2772.
15. Qi X, Fan J, Zhu J, Ling Y, Mi S, Chen H, et al. Circulating chemerin level and risk of cancer: a systematic review and meta-analysis. Biomark Med. 2020;14:919–28.
16. Rourke JL, Dranse HJ, Sinal CJ. Towards an integrative approach to understanding the role of chemerin in human health and disease. Obes Rev. 2013;14:245–62.
17. Hallahan AR, Pritchard JI, Hansen S, Benson M, Stoeck J, Hatton BA, et al. The SmoA1 mouse model reveals that notch signaling is critical for the growth and survival of sonic hedgehog-induced medulloblastomas. Cancer Res. 2004;64:7794–800.
18. Accelrys. Discovery Studio 3.1. 2011; 3.1:[Available from: http://accelrys.com].
19. Laskowski RA, Rullmannn JA, MacArthur MW, Kaptein R, Thornton JM. AQUA and PROCHECK-NMR: programs for checking the quality of protein structures solved by NMR. J Biomol NMR. 1996;8:477–86.
20. Huang J, Rauscher S, Nawrocki G, Ran T, Feig M, de Groot BL, et al. CHARMM36m: an improved force field for folded and intrinsically disordered proteins. Nat Methods. 2017;14:71–73.
21. Li L, Chen R, Weng Z. RDOCK: refinement of rigid-body protein docking predictions. Proteins. 2003;53:693–707.
22. Pettersen EF, Goddard TD, Huang CC, Couch GS, Greenblatt DM, Meng EC, et al. UCSF chimera - A visualization system for exploratory research and analysis. J Comput Chem. 2004;25:1605–12.
23. Zhang Y, Wang T, Wang S, Xiong Y, Zhang R, Zhang X, et al. Nkx2-2as suppression contributes to the pathogenesis of Sonic Hedgehog MB. Cancer Res. 2018;78:962–73.
24. Pietrobono S, Franci L, Imperatore F, Zanini C, Stecca B, Chiariello M. MAPK15 Controls Hedgehog Signaling in Medulloblastoma Cells by Regulating Primary Ciliogenesis. Cancers. 2021;13:4903.
25. Gupta K, Jogunoori S, Satapathy A, Salunke P, Kumar N, Radotra BD, et al. Medulloblastoma with myogenic and/or melanotic differentiation does not align immunohistochemically with the genetically defined molecular subgroups. Hum Pathol. 2018;75:26–33.
26. Carper MB, Denvir J, Boskovic G, Primerano DA, Claudio PP. RGS16, a novel p53 and pRb cross-talk candidate inhibits migration and invasion of pancreatic cancer cells. Genes Cancer. 2014;5:420–35.
27. Zhang Q, Jiang J. Regulation of Hedgehog signal transduction by ubiquitination and deubiquitination. Int J Mol Sci. 2021;22:13338.
28. Duman-Scheel M, Weng L, Xin S, Du W. Hedgehog regulates cell growth and proliferation by inducing Cyclin D and Cyclin E. Nature. 2002;417:299–304.
29. Sigafoos AN, Paradise BD, Fernandez-Zapico ME. Hedgehog/GLI signaling pathway: transduction, regulation, and implications for disease. Cancers. 2021;13:3410.
30. Lee C, Yi J, Park J, Ahn B, Won YW, Jeon J, et al. Hedgehog signalling is involved in acquired resistance to KRAS(G12C) inhibitors in lung cancer cells. Cell Death Dis. 2024;15:56.
31. Lospinoso Severini L, Loricchio E, Navacci S, Basili I, Alfonsi R, Bernardi F, et al. SALL4 is a CRL3(REN/KCTD11) substrate that drives Sonic Hedgehog-dependent medulloblastoma. Cell Death Differ. 2024;31:170–87.
32. Zeng LH, Tang C, Yao M, He Q, Qv M, Ren Q, et al. Phosphorylation of human glioma-associated oncogene 1 on Ser937 regulates Sonic Hedgehog signaling in medulloblastoma. Nat Commun. 2024;15:987.
33. Drummond CJ, Hanna JA, Garcia MR, Devine DJ, Heyrana AJ, Finkelstein D, et al. Hedgehog pathway drives fusion-negative rhabdomyosarcoma initiated from non-myogenic endothelial progenitors. Cancer Cell. 2018;33:108–24.
34. Kong JH, Siebold C, Rohatgi R. Biochemical mechanisms of vertebrate hedgehog signaling. Development. 2019;146:dev166892.
35. Pöschl J, Koch A, Schüller U. Histological subtype of MB frequently changes upon recurrence. Acta Neuropathol. 2015;129:459–61.
36. Ramaswamy V, Taylor MD. MB: from myth to molecular. J Clin Oncol. 2017;35:2355–63.
37. Cavalli FMG, Remke M, Rampasek L, et al. Intertumoral heterogeneity within MB subgroups. Cancer Cell. 2017;31:737–54.
38. Zhang L, He X, Liu X, Zhang F, Huang LF, Potter AS, et al. Single-cell transcriptomics in MB reveals tumor-initiating progenitors and oncogenic cascades during tumorigenesis and relapse. Cancer Cell. 2019;36:302–18.
39. Zhang L, Noguchi YT, Nakayama H, Kaji T, Tsujikawa K, Ikemoto-Uezumi M, et al. The CalcR-PKA-Yap1 axis is critical for maintaining quiescence in muscle stem cells. Cell Rep. 2019;29:2154–63.
40. Park AK, Lee JY, Cheong H, Ramaswamy V, Park SH, Kool M, et al. Subgroup-specific prognostic signaling and metabolic pathways in pediatric MB. BMC Cancer. 2019;19:571.
41. Zhu F, Wang P, Kontrogianni-Konstantopoulos A, Konstantopoulos K. Prostaglandin (PG)D(2) and 15-deoxy-Delta(12,14)-PGJ(2), but not PGE(2), mediate shear-induced chondrocyte apoptosis via protein kinase A-dependent regulation of polo-like kinases. Cell Death Differ. 2010;17:1325–34.
42. Fischer TF, Beck-Sickinger AG. Chemerin - exploring a versatile adipokine. Biol Chem. 2022;403:625–42.
43. Mattern A, Zellmann T, Beck-Sickinger AG. Processing, signaling, and physiological function of chemerin. IUBMB Life. 2014;66:19–26.
44. Treeck O, Buechler C, Ortmann O. Chemerin and cancer. Int J Mol Sci. 2019;20:3750.
45. Kumar JD, Kandola S, Tiszlavicz L, Reisz Z, Dockray GJ, Varro A. The role of chemerin and ChemR23 in stimulating the invasion of squamous oesophageal cancer cells. Br J Cancer. 2016;114:1152–9.
46. Erdmann S, Niederstadt L, Koziolek EJ, Gómez JDC, Prasad S, Wagener A, et al. CMKLR1-targeting peptide tracers for PET/MR imaging of breast cancer. Theranostics. 2019;9:6719–33.
47. Calebiro D, Grimes J. G protein-coupled receptor pharmacology at the single-molecule level. Annu Rev Pharm Toxicol. 2020;60:73–87.
48. Wireko AA, Ben-Jaafar A, Kong JSH, Mannan KM, Sanker V, Rosenke SL, et al. Sonic hedgehog signalling pathway in CNS tumours: its role and therapeutic implications. Mol Brain. 2024;17:83.

AUTHOR CONTRIBUTIONS

SW and TJ designed and performed major experiments and analyzed data. Tao Wang contributed to the sample collection and analysis. ZY performed molecular simulations and modeling study. Ting Wang and XZ participated in data collection. XG helped with manuscript organization and editing. LJ and LW analyzed the data and drafted the manuscript. YS designed the study and wrote the manuscript. All authors contributed to the article and approved the submitted version.

FUNDING

This work was financially supported by grant from the National Natural Science Foundation of China [82172910](LJ), Research Fund of Shaanxi Provincial Education Department [21JK0887](SW), Young Talent Fund of Association for Science and Technology in Shaanxi [20230303](SW), Shaanxi Innovative Research Team for Key Science and Technology [2022TD-47](LJ), and the Natural Science Basic Research Program of Shaanxi Province [2022JM-587](TW).

COMPETING INTERESTS

The authors declare no competing interests.

ETHICS APPROVAL

All animal study protocols were approved by the Institutional Animal Care and Use Committee (IACUC) of Fourth Military Medical University (Xi'an, China; protocol ID: 20220956). The use of clinical samples was in line with the principles of the Declaration of Helsinki, and approved by the Ethics Committee of Fourth Military Medical University (Xi'an, China; protocol ID: KY20224226).

ADDITIONAL INFORMATION

Supplementary information The online version contains supplementary material available at https://doi.org/10.1038/s41389-025-00582-1.

Correspondence and requests for materials should be addressed to Lintao Jia, Liang Wang or Yang Song.